The December 2015 Mount Etna eruption: an analysis of inflation/deflation phases and faulting processes

Marco Aloisi [1], Shuanggen Jin [2,3], Fabio Pulvirenti [2] and Antonio Scaltrito [1]

[1] Istituto Nazionale di Geofisica e Vulcanologia - Osservatorio Etneo, Catania 95125, Italy

[2] Shanghai Astronomical Observatory, Chinese Academy of Sciences, Shanghai 200030, China

[3] Department of Geomatics Engineering, Bulent Ecevit University, Zonguldak 67100, Turkey

Email: marco.aloisi@ingv.it (M. Aloisi); sgjin@shao.ac.cn (S. Jin); fabiopulvirenti@yahoo.it (F. Pulvirenti); antonio.scaltrito@ingv.it (A. Scaltrito)

Keywords: GPS; Ground deformation Modelling; Earthquakes; Mount Etna; Coulomb stress changes; Hydrothermal circulation; Inflation/deflation phases; Eruption;

Abstract

During the first days of December 2015, there were four paroxysmal events at the "Voragine" crater on Mount Etna, which were among the most violent observed during the last two decades. A few days after the "Voragine" paroxysms, the Pernicana - Provenzana fault system, located near the crater area, underwent an intense seismic swarm with a maximum "local" magnitude M_L of 3.6.

This paper investigates the relationship between the eruptive phenomenon and the faulting process in terms of Coulomb stress changes. The recorded seismicity is compatible with a multicausal stress redistribution inside the volcano edifice, occurring after the four paroxysmal

episodes that interrupted the usual trend of inflation observed at Mt. Etna. The recorded seismicity falls within the framework of a complex chain of various and intercorrelated processes that started with the inflation preparing the “Voragine” magmatic activity. This was followed with the rapid deflation of the volcano edifice during the paroxysmal episodes. We determined that the recorded deflation was not the direct cause of the seismic swarm. In fact, the associated Coulomb stress change, in the area of seismic swarm, was of about -1 [bar]. Instead, the fast deflation caused the rarely observed inversion of dislocation in the eastern flank at the same time as intense hydrothermal activity that, consequently, underwent an alteration. This process probably reduced the friction along the fault. Then, the new phase of inflation, observed at the end of the magmatic activity, triggered the faulting processes.

1. Introduction

Mount Etna, the largest volcano in Europe, is situated on continental crust and its formation is probably related to the nearby subduction process of the Ionian slab under the Tyrrhenian plate [Gvirtzman and Nur, 1999]. The structural evolution of the volcanic edifice is the result of the action of volcanic sources combined with tectonic processes, characterized by the presence of important fault zones (Fig. 1). This study on a small part of this complex tectonic scenery will contribute to understanding how the movements between faults are related to each other and with magma dynamics. In particular, we estimated stress changes along the faults in the Pernicana - Provenzana fault system [Azzaro, 1999; Obrizzo et al., 2001; Palano et al., 2006; Guglielmino et al., 2011; Alparone et al., 2013] after the major eruptions occurring at the “Voragine” Crater (Fig. 1). This approach is supported by the evidence that many authors [e.g., Patanè et al., 2005; Feuillet et al., 2006; Mattia et al., 2007; Currenti et al., 2008; Aloisi et al., 2011a; Bonanno et al., 2011; Privitera et al., 2012; Gonzalez and Palano, 2014] determined that, at Mount Etna, the stress

triggered by the magmatic activities is transferred to the faults and redistributed among them. For example, Feuillet et al. [2006], after analyzing historical earthquakes in eastern Sicily and eruptions at Mt. Etna volcano, found that volcanic sources and active faults are mechanically coupled. Therefore, there is an ample evidence that magmatic and faulting processes can interact with each other by changing or perturbing the state of stress and, in turn, promoting or inhibiting earthquakes or eruptions. Moreover, it is well known that establishing the relationship between volcanic unrest at Etna and Pernicana fault system re-activation is a critical topic to understanding Etna mechanical behaviour [e.g., Currenti et al., 2012]. In fact, the Pernicana - Provenzana fault system is one of the most active tectonic systems of Mt. Etna and it plays an important role in the dynamic of the eastern flank of the volcano, being closely correlated to the local stress field induced by volcano-related processes [Alparone et al., 2013].

It is known that, when earthquakes or magmatic activities occur, the stress state of the medium is modified by an additional stress field [e.g., Dragoni et al., 1982; Privitera et al., 2012], referred to as Coulomb static stress changes (hereafter, CSC). Earthquakes and volcanic activity interaction is a fundamental challenge for today's studies, leading to a deeper understanding of earthquake sequences, clustering and aftershocks. Many authors [e.g., Thatcher and Savage, 1982; Reasenberg and Simpson, 1992; King et al., 1994; Harris, 1998; Nostro et al., 1998; Stein 1999; Hill et al., 2002; Marzocchi et al., 2002; Toda et al., 2002; Hyodo and Hirahara, 2004; Walter and Amelung, 2004; Feuillet et al., 2006; Calais et al., 2010; Xu et al., 2010; Toda et al., 2011; Pulvirenti et al., 2016] have demonstrated that the CSC quantity [measured in bar] can be regarded as an alteration of the "potentiality" of slip of the fault plane in response to the current stress state of the medium. In particular, when this quantity is positive, the movement on the fault plane is stimulated and earthquakes can be triggered. The minimum positive value of CSC to trigger an earthquake depends on the area where the fault is located because of the different rheological conditions. However, changes of about 0.1 bar are considered sufficient to trigger movements on

78 the fault plane, when the system is close to the critical state of failure [e.g., Bonanno et al., 2011;
79 Toda et al., 2011; Gonzalez and Palano, 2014; Pulvirenti et al., 2016].
80 In this paper, the relationship between the magmatic activities and the faulting process at Mount
81 Etna is investigated in terms of CSC, in the area of the Pernicana - Provenzana fault system. We
82 developed an analytical model to study the deformation pattern of the Etna volcano during the
83 eruptive episodes occurring in December 2015. Therefore, the relationship between the inflation
84 recorded prior to the magmatic activity, the sudden ensuing volcano deflation recorded during the
85 December 2015 eruptive episodes, the starting of a successive new phase of inflation and the
86 following faulting processes observed along the Pernicana - Provenzana fault system, are
87 investigated in terms of CSC. Results indicated that, in a chain of various factors, only the new
88 inflation phase following the eruptive episodes is correlated to positive Coulomb stress changes in
89 the Pernicana - Provenzana fault system (Fig. 1), in accordance with the location, depth and focal
90 mechanism of the recorded seismic swarm. In Section 2, the tectonic setting and 2015 eruption are
91 introduced, a description of the recorded seismic activities and of the ground deformation modelling
92 are presented in Sections 3 and 4, respectively, and, finally, discussions and conclusions are given
93 in Sections 5 and 6.
94
95
96 **2. Tectonic setting and the December 2015 eruption**
97
98 Mount Etna is a basaltic strato-volcano located in the eastern coast of Sicily (Italy). It lies along
99 the front of the collision belt between the African and the Eurasian plates. Like many other
100 volcanoes in the world [Ellis and King, 1991], Mount Etna has arisen from the flank of a normal
101 fault, the Malta Escarpment. This is a major normal fault system separating the Hyblaean foreland
102 from the thinned Ionian crust (Fig. 1). The Etnean volcanic activities have been interpreted as the
103 result of extensional processes correlated a) to the Siculo-Calabrian rift zone [e.g., Ellis and King,

104 1991] or b) to vertical movement of asthenospheric material during the rollback motion of the
105 Ionian slab under the Tyrrhenian plate [e.g., Gvirtzman and Nur, 1999]. The volcano is subject to a
106 roughly N-S striking compressive regime due to the convergence between the Ionian and
107 Tyrrhenian plates [e.g., Cocina et al., 1997; Barberi et al., 2000] and, contemporaneously, to an
108 extensional approximately WNW-ESE regime, associated to the Malta Escarpment dynamics [e.g.,
109 Ellis and King, 1991; Hirn et al., 1997]. Moreover, the volcanic edifice is also subject to the local
110 stress due to magma activities [e.g., Barberi et al., 2000]. The interaction between this very
111 articulated stress field at Mount Etna produces two kinematically distinct sectors: a) the western
112 flank that has scant morphological evidence of faulting or eruptive fracturing and, analyzing the
113 recorded ground deformation pattern, is a clear indicator of the volcano inflation/deflation phases,
114 and b) the eastern flank that is formed by several fault systems accommodating a near constant
115 seaward flank displacement whose origin is still fiercely debated [e.g., Palano et al., 2008; Palano et
116 al., 2009; Aloisi et al, 2011a; Chiocci et al., 2011; Cannavò et al., 2014; Mattia et al., 2015; Palano,
117 2016].

118 Mount Etna is characterized principally by two types of eruptions [e.g., Aloisi et al., 2009]: a)
119 summit strombolian eruptions, where magma intrudes through the central conduit system, and b)
120 dike-forming eruptions, when magma breaks out at the surface, bypassing the central conduit
121 system. Historically, most of the dike-forming intrusions ascend along two rift zones, a) the NE Rift
122 and b) the S Rift zone (Fig. 1). In this paper, we discuss the summit eruptions occurring in
123 December 2015 and their relationship with the following seismic activity recorded at the northern
124 end of the NE Rift, along the Pernicana - Provenzana fault system.

125 Starting from the 2nd of December 2015, four intense paroxysmal eruptive episodes occurred at
126 the central crater, known also as “Voragine” crater (Fig. 1). The volcanic activity was characterized
127 by tall lava fountains and by eruption columns, several kilometres high. SO_2 emissions, related to
128 the different paroxysms, were tracked above the eastern Mediterranean, Syria, Iraq and China areas.

129 The paroxysmal events were among the most violent to be observed at Mount Etna during the last
130 two decades.

131 In the past, the “Voragine” crater underwent two particularly intense paroxysms on 22 July
132 1998 and on 4 September 1999, with similar characteristics to those of the paroxysms recorded
133 during December 2015 (https://www.volcanodiscovery.com/italysvolcanoes/VOR95_99.html). In
134 particular, the episode in July 1998 was accompanied by fire-fountaining and tephra emission.
135 Successively, vigorous activity at the Voragine resumed in early August, with another paroxysmal
136 eruptive episode on the 6th. After this volcanic episode, the Voragine became active again in June
137 1999. From then on, the activity gradually increased, culminating in another paroxysm on 4
138 September 1999, similar but more violent to that of 22 July 1998. Successively, the Voragine
139 experienced several further episodes of vigorous activity during the weeks following the 4
140 September 1999 eruption, but none were of similar magnitude. Finally, further violent paroxysmal
141 episodes took place at the “Voragine” crater in February 1947, July-August 1960 and August 1989.

142 Concerning recent activity, there were modest and sporadic ash emissions at the “Voragine”
143 crater from August 2015. More significant volcanic activity started during the month of October
144 2015, when the opening of a vent, producing modest intra-crateric strombolian activities and
145 sporadic weak ash emissions, was observed. This activity continued during October and November
146 without substantial variations, although it showed an increase in frequency and intensity over time.
147 Since the 1st of December until about 13:00 UTC on the 2nd of December, the volcanic tremor
148 showed temporary episodes of unrest with oscillations in amplitude (Fig. 2a). The intra-crateric
149 strombolian activity became intense and recurrent. Successively, the volcanic tremor increased
150 progressively (Fig. 2a), culminating during the first hours of the 3rd of December, at about 02:20
151 UTC, with a violent paroxysmal episode that lasted approximately 40 minutes. The volcanic
152 activity consisted of tall lava fountains, some hundreds of meters high, and by an eruption column
153 about 10 km high (above the sea level). At the end of the first paroxysmal event, the strombolian
154 activities inside the “Voragine” crater continued. Weak ash emissions were observed at the New

155 Southeast Crater (NSEC) and at the North-East crater (NEC), see inset in Figure 1. A few hours
156 later, at about the 09:00 UTC on the 4th of December, the "Voragine" crater underwent a second
157 paroxysmal episode (Fig. 2a), lasting as long as the first episode. During this paroxysm, there were
158 frequent ash emissions at the NSEC. The volcanic tremor amplitude, namely the daily average of
159 the Root Mean Square (RMS) amplitude of the vertical component of seismic signal [e.g., McNut,
160 1991; Alparone et al., 2003; Di Grazia et al., 2006], remained high at the ESLN seismic station
161 (Fig. 2a). It reached a peak during the second paroxysm in the morning, which was higher than the
162 peak associated with the paroxysm of the 3rd of December. At about 20:35 UTC on the 4th of
163 December and at about 14:55 UTC on the 5th of December, the "Voragine" crater underwent two
164 more intense eruptive episodes. These two episodes had similar features and durations as the first
165 two eruptive paroxysms. Successively, the eruptive activity at the "Voragine" crater gradually
166 diminished. The ash emissions continued at the NSEC. At the end of the fourth paroxysmal episode,
167 the volcanic tremor amplitude remained high (Fig. 2a), for about 7 hour, when, at about 01:00 UTC
168 on the 6th of December, it increased rapidly. During this new phase, the volcanic tremor amplitude
169 remained almost constantly high during the time, until about 06:00 UTC on the 8th of December.
170 This phase was characterized by vigorous strombolian and effusive activities at the NSEC. The
171 NSEC was also affected by ash emission. As described before, from the 3rd of December, weak ash
172 emission had been observed at the NSEC and at the NEC. From the 7th of December, the NEC was
173 affected by sporadic strombolian activity. This phase ended on the 8th of December at about 05:00
174 UTC, when the volcanic tremor amplitude sharply decreased to roughly the value reached after the
175 fourth "Voragine" crater paroxysms (Fig. 2a). During the first hours of the 8th of December, also the
176 NSEC eruptive activity decreased rapidly together with the volcanic tremor amplitude but,
177 contemporaneously, the ash emissions at the NEC increased. During this last phase, the volcanic
178 tremor amplitude decreased slowly together with the observed volcanic activity. In particular, there
179 was a new increase of ash emission at the NEC from December 9 to 11. Finally, sporadic ash

emissions and weak explosive activities were observed at the “Voragine” crater, NSEC and NEC until the end of December.

3. December 2015 seismic activities

The Etna Permanent Network, managed by Istituto Nazionale di Geofisica e Vulcanologia, Osservatorio Etneo (INGV-OE), consists of 35 three-component digital seismic stations (Fig. 1). These stations are equipped with broadband (Trillium–Nanometrics, F_n=40 s) three-component sensors, with a dynamic range of 144 dB. Data are acquired and recorded locally with a digital frequency of 100 Hz, using the Nanometrics Trident Digital Systems (24 bits). These data are transmitted via satellite or radio to the data acquisition center of the INGV-OE, Catania. All the stations use the same base time, set by GPS time.

Earthquakes at Mt. Etna can be divided in two major groups: a) volcanic-tectonic earthquakes that are generated by regional tectonic stress, local stress induced by dike-forming intrusion, local stress due to slower inflating sources or by a mutual interaction between the previously described causes [e.g., Patanè et al., 2003; Gambino, 2016]; b) long-period events driven by stress changes caused by an intermittent degassing process occurring at depth [e.g., Cauchie et al., 2015]. Usually, volcanic-tectonic earthquakes occur mainly in the form of swarms, seldom exceeding magnitude 4 [Gambino, 2016].

Fig. 3 shows the seismicity recorded between August and December 2015. This seismicity belongs to the volcanic-tectonic typology and affected mostly the eastern sector of the volcano edifice. It is grouped in swarms in the area of Pernicana - Provenzana faults system, located near the crater area, and in the eastern flank, near the area of Zafferana town (Fig. 3). We focused on an intense seismic swarm occurring in the uppermost segment of the Pernicana - Provenzana fault system (Fig. 3 and inset). In particular, between the 7th and 10th of December 2015, about 100

earthquakes with local maximum magnitude M_L of 3.6 were recorded in this area. The swarm started by an event with M_L 2.6, on 7 December, but the main earthquakes took place in the morning of 8 December, with two events at 09:28 GMT (M_L=3.6) and at 10:53 GMT (M_L=3.2). Only 14 events of the swarm were located, since the low level of recorded magnitude rarely exceeded the value of M_L=2.0 (see inset in Fig. 3 and Table 1). The depth of the swarm was between 0 and 1.5 km, below the sea level.

Fig. 4 shows the daily earthquake rate and the associated cumulative strain release [e.g., Alparone et al., 2015] of the earthquakes located during the period 2014-2015. It is noteworthy that the Pernicana - Provenzana 2015 swarm produced the main seismic energy release during the last two years, on Mount Etna (Fig. 4a). Moreover, between August and December 2015, another minor swarm occurred in the area of Milo - Zafferana towns (Fig. 4b).

The events belonging to the Pernicana - Provenzana 2015 swarm were selected from the INGV-OE catalogue [Gruppo Analisi Dati Sismici, 2015]. The earthquakes were located using the Hypoellipse code [Lahr, 1989] and the 1D crustal velocity model proposed for Etna area by Hirn et al. [1991]. We also computed the focal mechanisms for five earthquakes (Figure 3 and Table 2). To this end, we selected only those events with at least ten first motion P-polarities and with sufficient station coverage on the focal sphere. We used the FPFIT code by Reasenberg and Oppenheimer [1985]. The focal mechanism of the main earthquake had the following parameters: strike 80°, dip 55°, rake -10°. Overall, the fault-plane solutions showed (Fig. 3) a trans-tensional faulting feature, with P-axes roughly NE-SW oriented and dipping from 30° to 59°. These focal mechanisms have a near EW striking nodal plane roughly resembling the geological fault traces along the Provenzana - Pernicana fault system. Our results were in agreement with other literature data [Barberi et al., 2004; Alparone et al., 2013] and with field observations.

4. Deformation observations and modelling

Continuous GPS (hereafter, CGPS) monitoring of ground deformations on Mt. Etna started in November 2000. The current network configuration includes 33 stations that cover the entire volcano edifice (Fig. 1). CGPS data collected by the Etnean network were processed with the GAMIT/GLOBK software with IGS (International GNNS Service) precise ephemerides and Earth orientation parameters from the International Earth Rotation and Reference Systems Service (IERS), [King and Bock, 2004; Jin and Park, 2006]. The precise baselines with uncertainty are obtained on a daily based solution.

We analyzed the CGPS data collected at Mt. Etna from June 2015 to July 2016, focusing in detail on December 2015, when Mt. Etna was undergoing intense volcanic and seismic activities. The December 2015 events occurred during the usual trend of volcano inflation (Fig. 2d). In particular, the increase in length of the baseline EMEG-ESLN showed clearly how the dynamic of the volcano inflation was active several months before the volcanic episodes. Conversely, during the four paroxysmal eruptive episodes occurred at the "Voragine" crater, from the 2nd to the 6th of December, the continuous CGPS network recorded a rapid deflation of the volcano that affected the entire edifice (Fig. 2d; Fig. 5a and b). It is noteworthy that this trend is evident also at the ECRI station (Fig. 2c and 5a and b). The ECRI station usually shows a horizontal movement toward East, in line with the dynamics of the near Pernicana fault, whereas, during the paroxysmal episodes and following the overall volcano deflation, the station showed a dislocation roughly toward South-West and the baseline ECOR-ECRI decreased in length (Fig. 2c). Successively, from the 7th of December, a new phase of inflation started (Fig. 2b, c and d), with a similar trend to the usual inflation affecting the volcano before the eruptive episodes (Fig. 2d).

We modelled the recorded deformation pattern associated with the rapid deflation phase, occurring between the 2nd and the 6th of December (Fig. 2 and 5), as induced by a pressure source acting inside the volcano. We used the entire CGPS network but we set a lower weight at the ECPN and EC10 stations because, in this case, they were both affected by local effects or instrumental

errors. We performed an analytical inversion of CGPS data, assuming the pressure source as a finite spherical magma body solution of Mctigue [1987], obtaining a plausible data fit (Fig. 5). Among the different analytical models published in literature, we chose this source model since it showed a good trade-off between the number of degrees of freedom and the obtained data fit. Moreover, unlike the inflation sources characterized by an elongated shape, deflation sources typically showed an almost spherical shape [Bruno et al., 2012]. We therefore retain that, in this case, a spherical source can represent the recorded deformation pattern well. The Mctigue [1987] pressure source is determined by five parameters: the coordinates "x_c", "y_c" and "z_c" of the sphere center, the radius "r" and the pressure "P" on the surface of the model. It is well known that there is a trade-off between the crustal strength, the source pressure and the related volume (e.g. Davis, 1986; Yang et al., 1988; Newman et al., 2006). Hence, we might obtain a considerable uncertainty on the estimation of source pressure if we do not know the correct rheology and plausible source volume. In order to estimate the model parameters, we performed an analytical inversion using the Genetic Algorithm [Goldberg, 1989] and, subsequently, the Pattern Search technique (Lewis and Torczon, 1999) and a Nonlinear Least Squares technique. To estimate the uncertainty of each optimized model parameter, we adopted a Jackknife re-sampling method [Efron, 1982]. We included the effects of the topography using the topographically corrected method of Williams and Wadge [2000]. The medium was supposed homogeneous and isotropic with a Young modulus of 75 GPa and a Poisson ratio of 0.25 [Aloisi et al., 2011a].

The final optimal solution for the deflation phase is shown in Figure 5 (c and d) and the parameters are reported in Table 3. The obtained source is located under the "Voragine" crater, where the four paroxysms occurred, at a depth of about 4.8 km, below the mean sea level. We calculated the volume change ΔV (Table 3) according to Tiampo et al. [2000], using a suitable value of the effective shear modulus μ for a hot volcanic region equal to 5 GPa [e.g., Bonafede et al., 1986; Davis, 1986; Bonaccorso et al., 2005]. We obtained a variation in volume of about -20 x 10^6 m^3 of magma for all the four paroxysms. It is noteworthy that the position of the December

2015 deflation source is compatible with the historical solutions found in literature (e.g., Aloisi et al., 2011a; Bruno et al., 2012). In particular, the deflation pressure sources are usually located along the western border of the high velocity zone found by Aloisi et al. [2002], just below the Central Crater area [Bruno et al., 2012]. This position is compatible with the path where the magma is thought to ascend, according to tomographic analysis [e.g., Aloisi et al., 2002]. Regarding the found depth of about 4.8 km below the mean sea level, this level is of primary importance because, considering its depth beneath the crater area (about 7 km), it corresponds approximately to the pressure of exsolution (180 MPa) and bubbles formation of Etnean magmas with a normal content in water (2%), [see Bruno et al., 2012].

5. Analysis, results and discussions

In this paper, we investigated the interaction between the volcanic sources at Mt. Etna and the active faults in terms of mechanical coupling, by examining how the perturbation of the state of stress can promote or inhibit the seismicity. Taking into account the fault location, geometry and rake for the 8th of December recorded seismicity, we analyzed the relationship between the "Voragine" 2015 magmatic activities, the prior inflation phase, the following inflation phase and the faulting process, in terms of CSC.

Taking into account the estimated focal mechanism for the mainshock, recorded on the 8th of December at 09:28 UTC (M_L=3.6), we calculated the CSC induced by the modelled deflation source. We found that the movement on the fault plane along the Pernicana - Provenzana system is clearly impeded (Fig. 6). This means that the deflation phase, produced by the four paroxysmal episodes at the "Voragine" crater, is not the direct cause of the seismic swarm recorded a few days after. By contrast, a direct link between volcanic and seismic activity has been demonstrated in other cases. For example, the seismic swarm occurring on the southeastern flank of Mt. Etna on the

310 9th of January 2001 was associated with the magmatic recharge preceding the Mt. Etna 2001
311 eruption [Gambino, 2016]. Also the 22 September 2002 Pernicana seismicity was associated with a
312 tensile mechanism occurring during the magma intrusion that preceded the lateral eruption a month
313 later [Currenti et al., 2012]. Or, the October 2002 Pernicana seismic swarm was directly correlated
314 to the dyke-forming intrusions occurring during the 2002-2003 Mt. Etna eruption [Pulvirenti et al.,
315 2016]. As in our case, there was not always a direct link between volcanic and seismic activity. For
316 example, the 2-3 April 2010 Pernicana seismic swarm was associated with the flank seaward
317 movement, extending the eastern sector of Mt Etna [Currenti et al., 2012]. Therefore, we think that
318 the December 2015 seismicity can be interpreted exclusively in the framework of a significant
319 interplay between various processes (Fig. 7).
320 Although almost within the limit of instrumental errors, it is worth noting that the baseline
321 ECOR-ECRI (Fig. 2c) showed an inversion of the usual kinematics during the paroxysmal episodes.
322 The length of the baseline ECOR-ECRI usually increases in time, according to the dislocation along
323 the Pernicana fault. Instead, during the "Voragine" eruptive episodes, the baseline decreased in
324 length. Therefore, we believe that the four violent paroxysms destabilized the area subject to the
325 seismic swarm.
326 Moreover, on examining three typical CGPS baselines (Fig. 2b), we can observe that, during
327 the four eruptive episodes and all crater activities, the CGPS network recorded a deflation (the
328 baseline length decreases). However, starting from the 7th of December, one day before the main
329 earthquake of the seismic swarm, the CGPS baselines began increasing in length. This means that
330 the CGPS network started to record a new typical inflation phase (Fig. 2d), very similar to the phase
331 of inflation that the volcano recorded before the "Voragine" eruptive episodes. In order to explain
332 this inflation, we can observe that the seismic tremor, just a few hours before the seismic swarm,
333 diminishes rapidly (Fig. 2a). We assumed, after the four paroxysmal episodes at the "Voragine"
334 crater and the activities observed at the NSEC and NEC craters, that the modelled deflation area
335 located at a depth of about 4.8 km (below the mean sea level) and the entire overlying plumbing

system were filled with less volatile-rich magma than the one erupted before. This observation, that corresponds to the decreasing concentration of dissolved volatiles and of the gas boiling, can explain the rapid drop in seismic tremor and the progressive decreasing of the observed volcanic activity. The volatiles that continuously rise through the magmas [Ferlito et al., 2009; Ferlito and Lanzafame, 2010], in the plumbing system, therefore now characterized by a low concentration of dissolved volatiles, can explain the beginning of the new phase of inflation. Our hypothesis here is that the content of volatiles in the new batch of magma, that filled the deflation area and the overlying plumbing system, increased in time after the eruptive activity, promoting the new inflation phase (Fig. 2d). In particular, we believe that the observed overpressure provided to the magma is associated to the gas exsolution and boiling. It is not possible to model the source of inflation between 7th and 8th of December, because we recorded very small displacements at the CGPS network, just beyond the instrumental error. The observed overpressure during one day was very small. If we hypothesize a positive variation in volume located at about 4.8 km, below the mean sea level, roughly matching with the depth and horizontal position of the previous source in deflation producing the here modelled 2015 “Voragine” volcanic activity, we obviously obtain positive CSC in correspondence with the recorded seismicity along the Pernicana - Provenzana fault system. Therefore, the recorded earthquakes could be compatible with the starting of a new phase of inflation and, probably, the previous rapid deflation produced a state of disequilibrium in the studied area (Fig. 7). Likewise, as aforementioned, the seismic swarm on the southeastern flank of Mt. Etna on the 9th of January 2001 represented a shear response to a local stress caused by the magmatic recharge preceding the Mt. Etna 2001 eruption [Gambino, 2016]. It was determined that the 9th of January fault reactivation occurred along pre-existing structures, most likely, because of the presence of fluids. In fact, Siniscalchi et al. [2012], by means of magnetotelluric survey on the eastern flank of Mt. Etna, have detected several high conductivity zones, suggesting diffuse hydrothermal activity and fluid circulation. In particular, the authors deduced that the zone with the strongest conductivity lies in the intensely fractured hanging wall of the Pernicana fault system (see

362 also Siniscalchi et al., 2010). Therefore, the area where the December 2015 swarm occurred is
363 affected by intense hydrothermal activity, fluid circulation and convective hydrothermal cells, able
364 to induce instability (Fig. 7). During the “Voragine” magmatic activity - among the most violent
365 observed during the last two decades - the entire eastern flank, that is usually characterized by a
366 continuous seaward movement (Fig. 7a) [e.g., Bonforte and Puglisi, 2006; Bonforte et al., 2007;
367 Battaglia et al., 2011; Chiocci et al., 2011; Apuani et al., 2012; Acocella and Puglisi, 2013; Ruch et
368 al., 2013], was dislocated in just a few days toward the crater area (Fig. 5a and 7b). This event of a
369 reversal dislocation is very rarely [Aloisi et al., 2011b; Bruno et al., 2012] and, in this case, it was
370 very fast (Fig. 7). It is well know that the Pernicana - Provenzana fault system represents the
371 northern edge of the eastern flank (Fig. 5a) and, beyond this margin toward the north, the motion of
372 the flank abruptly disappears [e.g., Bonforte and Puglisi, 2006; Bonforte et al., 2011; Barreca et al.,
373 2013; Ruch et al., 2013]. It is almost certain that the inversion of dislocation at the eastern flank
374 must have produced an alteration of the hydrothermal circulation, in particular, in the northern and
375 western edge of the flank (Fig. 7b). This evidence could indicate a reduction of the effective normal
376 stress along the Pernicana - Provenzana fault system, induced indirectly by the very fast deflation
377 associated to the “Voragine” paroxysmal episodes. In confirmation of this hypothesis, also Mattia et
378 al. [2015] pointed to the crucial interrelationship between fluids of volcanic origin and aquifers,
379 producing the large scale instability of the eastern flank of Mt. Etna. The authors clearly
380 demonstrated that the strain patterns related to the action of volcanic sources (inflation/deflation
381 cycles) influence the pore pressure of the shallower layers, inducing movements in the eastern flank
382 and, consequently, changing the shallow depth fluid circulation. The close correlation between
383 magma emplacement within the North East Rift, the amount of deformation near the Pernicana fault
384 system and the instability of the eastern flank of Mt. Etna has already been discussed by many
385 authors (e.g., Ruch et al., 2013). In our case, it is noteworthy that typical baselines on the eastern
386 flank near the studied area, for example, the ESAL-ERIP and EMFN-EBAG baselines (Fig. 2c),
387 indicated that until about the 6th of December they increased in length according to the overall

388 volcano deflation due to the “Voragine” paroxysmal episodes. From about the 6th of December,
389 when the “Voragine” magmatic activity finished, the trend recorded at the two baselines changed,
390 indicating the resumption of the typical flank seaward movement (Fig. 7b). In conclusion, the 2015
391 December seismic activity was the consequence of a mosaic of volcanic and tectonic processes. We
392 believe that the “Voragine” paroxysmal episodes induced fast movements in the eastern flank
393 toward the craters area (Fig. 7b) and that the flank resumed its usual seaward movement after the 6th
394 of December. This process produced a variation in the fluid circulation with the consequent
395 reduction of the friction along the Pernicana - Provenzana fault system. Successively, the onset of
396 the new phase of inflation (Fig. 7c), producing a positive CSC along the fault system, triggered the
397 faulting processes, releasing the pre-stress cumulated during interseismic period (Fig. 7a), as the
398 consequence of the intrusive dynamics preceding the “Voragine” magmatic activity.
399
400
401 **6. Conclusions**
402
403 In this paper, the relationship between the eruptive phenomenon and the faulting process in
404 terms of Coulomb stress changes has been investigated. Our study determined that the four
405 paroxysmal episodes at the “Voragine” crater are not the direct cause of the seismic swarm recorded
406 a few days later. We also demonstrated that the violent magmatic activity destabilized this area,
407 promoting a fast inversion of dislocation in the eastern flank and a consequent variation in the fluid
408 circulation (Fig. 7b). Therefore, due to the presence of intense hydrothermal activity, the rapid
409 deflation indirectly caused a weakening of the failure surface that was successively activated by the
410 start of the new phase of inflation (Fig. 7c). In fact, our results of the inflation phase following the
411 2015 December eruptive episodes indicated positive Coulomb stress changes in the Pernicana -
412 Provenzana fault system, in accordance with the location, depth and focal mechanisms of the

recorded seismic swarm. Given this match, we can conclude that the recorded seismicity is compatible with a complex and multicausal stress redistribution inside the volcano edifice (Fig. 7).

Table 1 - Main hypocentral parameters of the localized events

N	Date	Origin Time	Lat	Long	Depth [km]	M_L	Area
1	07/12/2015	19.12.20	37.8079	15.0510	0.02	2.6	1.8 km W from Piano Pernicana (CT)
2	08/12/2015	09.28.30	37.8037	15.0453	1.26	3.6	1.5 km E from Monte Nero (CT)
3	08/12/2015	09.32.03	37.8125	15.0538	0.82	2.7	1.7 km W from Piano Pernicana (CT)
4	08/12/2015	09.36.22	37.8113	15.0455	0.93	2.3	1.4 km E from Monte Nero (CT)
5	08/12/2015	09.56.00	37.8039	15.0412	1.11	1.7	1.2 km SE from Monte Nero (CT)
6	08/12/2015	10.22.37	37.8021	15.0395	1.24	1.4	1.2 km SE from Monte Nero (CT)
7	08/12/2015	10.53.54	37.8024	15.0434	1.5	3.2	1.4 km SE from Monte Nero (CT)
8	08/12/2015	14.55.57	37.7968	15.0278	1.29	1.3	1.4 km S from Monte Nero (CT)
9	08/12/2015	20.06.25	37.8081	15.0462	0.36	2.1	1.4 km E from Monte Nero (CT)
10	08/12/2015	20.50.37	37.8028	15.0415	1.98	1.3	1.3 km SE from Monte Nero (CT)
11	08/12/2015	20.51.15	37.8077	15.0555	1.22	1.6	1.4 km W from Piano Pernicana (CT)
12	09/12/2015	01.27.09	37.8020	15.0365	1.11	1.2	1.0 km SE from Monte Nero (CT)
13	09/12/2015	08.14.29	37.8078	15.0429	1.05	2.1	1.2 km E from Monte Nero (CT)
14	10/12/2015	04.43.29	37.7973	15.0296	1.55	1.6	1.3 km S from Monte Nero (CT)

Table 2 – Estimated focal parameters (numeration from Tab. 1)

N	Date	Origin Time	Lat	Long	Depth [km]	M_L	Strike	Dip	Rake	Area
1	07/12/2015	19:12:20	37.8079	15.051	0.02	2.6	170	60	-160	1.8 km W from Piano Pernicana (CT)
2	08/12/2015	09:28:30	37.8037	15.0453	1.26	3.6	80	55	-10	1.5 km E from Monte Nero (CT)
3	08/12/2015	09:32:03	37.8125	15.0538	0.82	2.7	60	65	-60	1.7 km W from Piano Pernicana (CT)
4	08/12/2015	09:36:22	37.8113	15.0455	0.93	2.3	95	70	-30	1.4 km E from Monte Nero (CT)
7	08/12/2015	10.53.54	37.8024	15.0434	1.5	3.2	90	55	-50	1.4 km SE from Monte Nero (CT)

Table 3 - Model parameters and related uncertainties. ΔV is calculated according to Tiampo et al. (2000) using a value of the effective shear modulus μ equal to 5GPa

x_c [m]	499604 ± 85
y_c [m]	4178354 ± 102
z_c [m]	-4840 ± 248
r [m]	288 ± 69
P [Pa]	$-1.3 \times 10^9 \pm 2.5 \times 10^7$
ΔV $[m^3]$	$-20 \times 10^6 \pm 15 \times 10^6$

Caption

Fig. 1 - Map of Mount Etna with the continuous CGPS network (inverted triangles) and seismic network (circles), run by INGV-OE. A sketch map of the fault systems is reported, together with the NE and South rift zones. In the inset a), the location of Mount Etna in the central Mediterranean area is shown at the footwall of the Malta Escarpment. In the inset b), the crater area is shown in detail. The inset c) shows the consensus magma pathways, as historically resolved by GPS, seismic, and other geophysical data. Redrawn from Aloisi et al. [2011a].

Fig. 2 - (a) RMS of the seismic signal recorded at the ESLN station from 1 to 9 December 2015. (b) Length variation of three CGPS baselines (EMEG-ESLN, EMEG-ECPN, EMEG-EINT) located in the western flank of Etna volcano, from 1 to 9 December. (c) Length variation of one CGPS baseline (ECOR-ECRI) located across the Pernicana fault, from 1 to 9 December. The data clearly show the sudden variations related to the fast deflation recorded during the four paroxysms (from 2 to 6 December). The starting of a new phase of inflation during 7-8 December can also be seen. Two CGPS baselines (ESAL-ERIP and EMFN-EBAG) located on the eastern flank are also

reported. (d) Length variation of the CGPS baseline EMEG-ESLN for a long period (from June 2015 to July 2016). (e) Map of Mount Etna showing the plotted baselines.

Fig. 3 - Spatial distribution of the seismicity recorded between August and December 2015. In the inset, the 2-10 December seismicity and the principal focal mechanisms are shown.

Fig. 4 - Number of earthquakes per day (grey bars) and cumulative curve of seismic strain release (blue line) associated to the period 2014-2015 (a) and a detail (dashed red line) relative to the period between August and December 2015 (b).

Fig. 5 - a) Recorded (blue arrows) and modelled (red arrows) horizontal displacement field from 2 to 6 December. The mean uncertainty is of about 2.0-2.3 [mm]. b) The histogram reports the recorded (blue bars) and modelled (red bars) vertical dislocations. The vertical variations are sorted by the CGPS station elevations. The position of the modelled volcanic source in deflation (cyan circle) is also reported in horizontal c) and vertical d) projection. The red star in a) indicates the main earthquake recorded during 8 December 2015. The consensus magma pathways (black asterisks) as historically resolved by GPS, seismic and other geophysical data are indicated in c) and d) (see Aloisi et al. [2011a] for an overview). The trace of the high v_p body estimated by Aloisi et al. [2002] is also shown in c) and d).

Fig. 6 - Map of the Coulomb stress changes induced by the modelled deflation source and resolved on the receiver fault strike (80°, dip 55°, rake -10°) estimated for the mainshock (8^{th} of December at 09:28 UTC, M_L=3.6), at the depth of 1.26 km (b.s.l.), namely the hypocentral depth of the earthquake. The star indicates the main recorded earthquake (M_L=3.6) and the circle the modelled volcanic source. The seismic swarm is also reported.

Fig. 7 - Sketch map showing the volcanic and tectonic processes leading to the 2015 December seismic activity. a) Inflation phase recorded before the “Voragine” paroxysmal episodes, from June 2015 until the 2nd of December 2015. b) “Voragine” paroxysmal episodes, from 2 to 6 December 2015. c) Onset of a new phase of inflation, promoting the faulting processes, from 7 to 10 December 2015.

References

Acocella, v., Puglisi, G., 2013. How to cope with volcano flank dynamics? A conceptual model behind possible scenarios for Mt. Etna, Journal of Volcanology and Geothermal Research, Volume 251, Pages 137-148, ISSN 0377-0273, doi: 10.1016/j.jvolgeores.2012.06.016.

Aloisi, M., Cocina, O., Neri, G., Orecchio, B., Privitera, E., 2002. Seismic tomography of the crust underneath the Etna volcano, Sicily, Phys. Earth Planet. Inter., 134, 139–155, doi:10.1016/S0031-9201(02) 00153-X.

Aloisi, M., Bonaccorso, A., Cannavò, F., Gambino, S., Mattia, M., Puglisi, G., Boschi, E. 2009. A new dike intrusion style for the Mount Etna May 2008 eruption modelled through continuous tilt and GPS data, Terra Nova, 21, 316–321, doi:10.1111/j.1365-3121.2009.00889.x.

Aloisi, M., Mattia, M., Monaco, C., Pulvirenti, F., 2011a. Magma, faults, and gravitational loading at Mount Etna: The 2002–2003 eruptive period. J. Geophys. Res., 116, B05203. doi:10.1029/2010JB007909.

Aloisi, M., Mattia, M., Ferlito, C., Palano, M., Bruno, V., Cannavò, F., 2011b. Imaging the multi-level magma reservoir at Mt. Etna volcano (Italy), Geophys. Res. Lett., 38, L16306, doi:10.1029/2011GL048488.

Alparone, S., Andronico, D., Lodato, L., Sgroi, T., 2003. Relationship between tremor and volcanic activity during the Southeast Crater eruption on Mount Etna in early 2000, J. Geophys. Res., 108, 2241, doi:10.1029/2002JB001866.

Alparone, S., Cocina, O., Gambino, S., Mostaccio, A., Spampinato, S., Tuvè, T., Ursino, A., 2013. Seismological features of the Pernicana–Provenzana fault system (Mt Etna, Italy) and implications for the dynamics of northeastern flank of the volcano, J. Volcanol. Geotherm. Res., 251, 16–26, doi: 10.1016/j.jvolgeores.2012.03.010.

Alparone, S., Maiolino, V., Mostaccio, A., Scaltrito, A., Ursino, A., Barberi, G., D'Amico, S., Di Grazia, G., Giampiccolo, E., Musumeci, C., Scarfì, L., Zuccarello, L., 2015. Instrumental seismic catalogue of Mt Etna earthquakes (Sicily, Italy): ten years (2000-2010) of instrumental recordings, "Annals of Geophysics", 58, 4, S0435; doi:10.4401/ag-6591.

Apuani, T., Corazzato, C., Merri, A., Tibaldi, A., 2013. Understanding Etna flank instability through numerical models, Journal of Volcanology and Geothermal Research, Volume 251, Pages 112-126, ISSN 0377-0273, doi: 10.1016/j.jvolgeores.2012.06.015.

Azzaro, R., 1999. Earthquake surface faulting at Mount Etna volcano (Sicily) and implications for active tectonics, Journal of Geodynamics, Volume 28, Issues 2–3, Pages 193-213, ISSN 0264-3707, doi: 10.1016/S0264-3707(98)00037-4.

Barberi, G., Cocina, O., Neri, G., Privitera, E., Spampinato, S., 2000. Volcanological inferences from seismic strain tensor computations at Mt. Etna Volcano, Sicily, Bull. Volcanol., 62, 318 – 330.

Barberi, G., Cocina, O., Maiolino, E., Musumeci, C., Privitera , E., 2004. Insight into Mt. Etna (Italy) kinematic during the 2002-2003 eruption as inferred from seismic stress and strain tensors. Geophysical Research Letters 31, L21614. Doi: 10.1029/2004GL020918.

Barreca, G., Bonforte, A., Neri, M., 2013. A pilot GIS database of active faults of Mt. Etna (Sicily): A tool for integrated hazard evaluation, Journal of Volcanology and Geothermal Research, Volume 251, Pages 170-186, ISSN 0377-0273, doi: 10.1016/j.jvolgeores.2012.08.013.

520 Battaglia, M., Di Bari, M., Acocella, V., Neri, M., 2011. Dike emplacement and flank instability
521 at Mount Etna: Constraints from a poro-elastic-model of flank collapse, Journal of Volcanology and
522 Geothermal Research, Volume 199, Issues 1–2, Pages 153-164, ISSN 0377-0273, doi:
523 10.1016/j.jvolgeores.2010.11.005.
524 Bonaccorso A., Cianetti S., Giunchi C., Trasatti E., Bonafede M. and E. Boschi, 2005.
525 Analytical and 3D numerical modeling of Mt. Etna (Italy) volcano inflation. Geophys. J. Int. 163
526 (2), 852–862. doi:10.1111/j.1365-246X.2005.02777.x.
527 Bonafede M., Dragoni M. and F. Quareni, 1986. Displacement and stress fields produced by a
528 centre of dilation and by a pressure source in a viscoelastic half-space: application to the study of
529 ground deformation and seismic activity at Campi Flegrei, Italy. Geophys. J. R. Astron. Soc. 87,
530 455–485.
531 Bonanno, A., Palano, M., Privitera, E., Gresta, S., Puglisi, G., 2011. Magma intrusion
532 mechanisms and redistribution of seismogenic stress at Mt. Etna volcano (1997-1998). Terra Nova,
533 23, 339-348, doi:10.1111/j.1365-3121.2011.01019.x, 2011.
534 Bonforte, A., Puglisi, G., 2006. Dynamics of the eastern flank of Mt. Etna volcano (Italy)
535 investigated by a dense GPS network, Journal of Volcanology and Geothermal Research, Volume
536 153, Issues 3–4, Pages 357-369, ISSN 0377-0273, doi: 10.1016/j.jvolgeores.2005.12.005.
537 Bonforte, A., Branca, S., Palano, M., 2007. Geometric and kinematic variations along the active
538 Pernicana fault: Implication for the dynamics of Mount Etna NE flank (Italy), Journal of
539 Volcanology and Geothermal Research, Volume 160, Issues 1–2, Pages 210-222, ISSN 0377-0273,
540 doi: 10.1016/j.jvolgeores.2006.08.009.
541 Bonforte, A., Guglielmino, F., Coltelli, M., Ferretti, A., Puglisi, G., 2011. Structural assessment
542 of Mount Etna volcano from Permanent Scatterers analysis, Geochem. Geophys. Geosyst., 12,
543 Q02002, doi:10.1029/2010GC003213.

544 Bruno, V., Mattia, M., Aloisi, M., Palano, M., Cannavò, F., Holt, W.E., 2012. Ground
545 deformations and volcanic processes as imaged by CGPS data at Mt. Etna (Italy) between 2003 and
546 2008. Journal of Geophysical Research – Solid Earth, 117, B07208, doi:10.1029/2011JB009114.
547 Calais, E., Freed, A., Mattioli, G., Amelung, F., J´onsson, S., Jansma, P., Hong, S.H., Dixon, T.,
548 Prepetit, C., Momplaisir, R., 2010. The January 12, 2010, Mw 7.0 earthquake in Haiti: context and
549 mechanism from an integrated geodetic study, Nature Geosciences, doi 10.1038/NGEO992.
550 Cannavó, F., Arena, A., Monaco, C., 2014. Local geodetic and seismic energy balance for
551 shallow earthquake prediction. Journal of Seismology, 1-8. doi: 10.1007/s10950-014-9446-z.
552 Cauchie, L., Saccorotti, G., Bean, C. J., 2015. Amplitude and recurrence time analysis of LP
553 activity at Mount Etna, Italy, J. Geophys. Res. Solid Earth, 120, 6474–6486,
554 doi:10.1002/2015JB011897.
555 Chiocci, F.L., Coltelli, M., Bosman, A., Cavallaro D. 2011. Continental margin large-scale
556 instability controlling the flank sliding of Etna volcano. Earth and Planetary Science Letters,
557 Volume 305, Issues 1-2, 1 May 2011, Pages 57-64. doi: 10.1016/j.epsl.2011.02.040.
558 Cocina, O., Neri, G., Privitera, E., Spampinato, S., 1997. Stress tensor computations in the
559 Mount Etna area (southern Italy) and tectonic implications, J. Geodyn., 23, 109–127,
560 doi:10.1016/S0264-3707(96)00027-0.
561 Currenti, G., Del Negro, C., Ganci, G., Williams, C.A., 2008. Static stress changes induced by
562 the magmatic intrusions during the 2002-2003 Etna eruption. J. Geophys. Res. 113, B10206.
563 doi:10.1029/2007JB005301.
564 Currenti, G., Solaro, G., Napoli, R., Pepe, A., Bonaccorso, A., Del Negro, C., Sansosti, E.,
565 2012. Modeling of ALOS and COSMO-SkyMed satellite data at Mt Etna: Implications on relation
566 between seismic activation of the Pernicana fault system and volcanic unrest, Remote Sensing of
567 Environment, Volume 125, Pages 64-72, ISSN 0034-4257, doi: 10.1016/j.rse.2012.07.008.

568 Davis P. M., 1986. Surface deformation due to inflation of an arbitrarily oriented triaxial
569 ellipsoidal cavity in an elastic half-space, with reference to Kilauea Volcano, Hawaii, J. Geophys.
570 Res., 91(B7), 7429–7438, doi:10.1029/JB091iB07p07429.
571 Di Grazia, G., Falsaperla, S., Langer, H., 2006. Volcanic tremor location during the 2004 Mount
572 Etna lava effusion, Geophys. Res. Lett., 33, L04304, doi:10.1029/2005GL025177.
573 Dragoni, M., Bonafede, M., Boschi, E., 1982. Stress relaxation in the Earth and seismic activity,
574 Rivista del Nuovo Cimento, 5, 2, 1–34. doi: 10.1007/BF02740828.
575 Efron B., 1982. The Jackknife, Bootstrap and Other Resampling Plans. Society for Industrial
576 and Applied Mathematics, Philadelphia.
577 Ellis, M., King, G. 1991. Structural control of flank volcanism in continental rifts, Science, 254,
578 839–842, doi:10.1126/science.254.5033.839.
579 Ferlito, C., Viccaro, M., Cristofolini, R., 2009. Volatile‐rich magma injection into the feeding
580 system during the 2001 eruption of Mt. Etna (Italy): Its role on explosive activity and change in
581 rheology of lavas, Bull. Volcanol., 71, 1149–1158, doi:10.1007/s00445-009-0290-x.
582 Ferlito, C., Lanzafame, G., 2010. The role of supercritical fluids in the potassium enrichment of
583 magmas at Mount Etna volcano (Italy), Lithos, 119, 642–650, doi:10.1016/j.lithos.2010.08.006.
584 Feuillet, N., Cocco, M., Musumeci, C., Nostro, C., 2006. Stress interaction between seismic
585 and volcanic activity at Mt. Etna. Geophys. J. Int., 164, 697–718. doi:10.1111/j.1365-
586 246X.2005.02824.x.
587 Gambino, S. 2016. Tilt offset associated with local seismicity: the Mt. Etna January 9, 2001
588 seismic swarm.. Open Geosciences, 8(1), pp. 514-522. doi:10.1515/geo-2016-0045.
589 Goldberg D.E., 1989. Genetic Algorithms in Search, Optimization and Machine Learning.
590 Kluwer Academic Publishers, Boston, MA.
591 Gonzalez, P. J., Palano, M., 2014. Mt. Etna 2001 eruption: New insights into the magmatic
592 feeding system and the mechanical response of the western flank from a detailed geodetic dataset.

593 Journal of Volcanology and Geothermal Research, 274, 108–121. doi:
594 10.1016/j.jvolgeores.2014.02.001.
595 Gruppo Analisi Dati Sismici, 2016. Catalogo dei terremoti della Sicilia Orientale - Calabria
596 Meridionale (1999-2016), INGV, Catania http://www.ct.ingv.it/ufs/analisti/catalogolist.php.
597 Guglielmino, F., Bignami, C., Bonforte, A., Briole, P., Obrizzo, F., Puglisi, G., Stramondo, S.,
598 Wegmüller, U., 2011. Analysis of satellite and in situ ground deformation data integrated by the
599 SISTEM approach: The April 3, 2010 earthquake along the Pernicana fault (Mt. Etna - Italy) case
600 study. Earth and Planetary Science Letters, Volume 312, Issues 3–4, Pages 327-336, ISSN 0012-
601 821X, doi: 10.1016/j.epsl.2011.10.028.
602 Gvirtzman, Z., Nur, A., 1999. The formation ofMount Etna as the consequence of slab rollback.
603 Nature 401, 782-785, doi:10.1038/44555.
604 Harris R.A., 1998. Introduction to Special Section: Stress Triggers, Stress Shadows, and
605 Implications for Seismic Hazard. Journal of Geophysical Research, 103, B10, 24,347-24,358. doi:
606 10.1029/98JB01576.
607 Hill, D. P., Pollitz, F., Newhall, C., 2002. Earthquake-volcano interactions, Physics Today, 55,
608 41–47. doi: 10.1063/1.1535006.
609 Hirn, A., Nercessian, A., Sapin, M., Ferrucci, F., Wittlinger, G., 1991. Seismic heterogeneity of
610 Mt Etna: structure and activity, Geophys. J. Int., 105, 139-153.
611 Hirn, A., Nicolich, R., Gallart, J., Laigle, M., Cernobori, L., ETNASEIS Scientific Group, 1997.
612 Roots of Etna volcano in faults of great earthquakes, Earth Planet. Sci. Lett., 148, 171–191,
613 doi:10.1016/S0012-821X(97)00023-X.
614 Hyodo, M., Hirahara, K., 2004. GeoFEM Kinematic earthquake cycle simulation in Southwest
615 Japan. Pure and Applied Geophysics, 164, 2069-2090. Doi: 10.1007/s00024-004-2549-7.
616 Jin, S.G., Park, P.K., 2006. Strain accumulation in South Korea inferred from GPS
617 measurements, Earth Planets Space, 58(5), 529-534, doi: 10.1186/BF03351950.

King, G.C.P., Stein R.S., Lin, J., 1994. Static stress changes and the triggering of earthquakes, Bull. Seismol. Soc. Am., 84, 935-953.

King, R., Bock, Y., 2004. Documentation for the MIT GPS analysis software: GAMIT. Mass. Inst. of Technol., Cambridge.

Lahr, J. C., 1989. HYPOELLIPSE/VERSION 2.0: A computer program for determining local earthquake hypocentral parameters, magnitude and first motion pattern, Open File Rep. 89-116, 92 pp., U. S. Geol. Surv., Washington.

Lewis R.M. and V. Torczon, 1999. Pattern search algorithms for bound constrained minimization, SIAM J. Optim. 9 (4), 1082–1099.

Marzocchi, W., Casarotti, E., Piersanti, A., 2002. Modeling the stress variations induced by great earthquakes on the largest volcanic eruptions of the 20th century. Journal of Geophysical Research, 107. doi: 10.1029/2001JB001391.

Mattia, M., Patanè, D., Aloisi, M. Amore, M., 2007. Faulting on the western flank of Mt Etna and magma intrusions in the shallow crust. Terra Nova, 19, 1-6, doi: 10.1111/j.1365-3121.2006.00724.x.

Mattia, M., Bruno, V., Caltabiano, T., Cannata, A., Cannavò, F., D'Alessandro, W., Di Grazia, G., Federico, C., Giammanco, S., La Spina, A., Liuzzo, M., Longo, M., Monaco, C., Patanè, D., Salerno, G., 2015. A comprehensive interpretative model of slow slip events on Mt. Etna's eastern flank, Geochem. Geophys. Geosyst., 16, doi:10.1002/2014GC005585.

McNutt, S. R., 1991. Volcanic tremor, in Encyclopedia of Earth System Science, vol. 4, p. 9, Academic, San Diego, Calif.

McTigue DF, 1987. Elastic stress and deformation near a finite sphericalmagma body: resolution of the point source paradox. J. Geophys. Res. 92, 12931–12940, doi: 10.1029/JB092iB12p12931.

642 Newman A. V., T. H. Dixon and N. Gourmelen, 2006. A four-dimensional viscoelastic
643 deformation model for Long Valley Caldera, California, between 1995-2000, J. Volc. Geotherm
644 Res., 150, 244-269, doi:10.1016/j.jvolgeores.2005.07.017.
645 Nostro, C., Stein, R. S., Cocco, M., Belardinelli, M.E., Marzocchi, W., 1998. Two-way coupling
646 between Vesuvius eruptions and southern Apennine earthquakes (Italy) by elastic stress transfer, J.
647 Geophys. Res., 103(B10), 24,487-24,504. doi: 10.1029/98JB00902.
648 Obrizzo, F., Pingue, F., Troise, C., De Natale, G., 2001. Coseismic displacements and creeping
649 along the Pernicana fault (Etna, Italy) in the last 17 years: a detailed study of a tectonic structure on
650 a volcano, Journal of Volcanology and Geothermal Research, Volume 109, Issues 1–3, Pages 109-
651 131, ISSN 0377-0273, doi: 10.1016/S0377-0273(00)00307-3.
652 Palano, M., Aloisi, M., Amore, M., Bonforte, A., Calvagna, F., Cantarero, M., Consoli, O.,
653 Consoli, S., Guglielmino, F., Mattia, M., Puglisi, B., Puglisi, G., 2006. Kinematics and strain
654 analyses of the eastern segment of the Pernicana fault (Mt. Etna, Italy) derived from geodetic
655 techniques (1997 - 2005). Annals of Geophysics, vol. 49, pp. 1105-1117, doi: 10.4401/ag-3103.
656 Palano, M., Puglisi, G., Gresta S., 2008. Ground deformation patterns at Mt. Etna from 1993 to
657 2000 from joint use of InSAR and GPS techniques, J. Volcanol. Geotherm. Res., 169, 99–120,
658 doi:10.1016/j.jvolgeores.2007.08.014.
659 Palano, M., Gresta, S., Puglisi, G., 2009. Time-dependent deformation of the eastern flank of
660 Mt. Etna: After-slip or viscoelastic relaxation? Tectonophysics, 473, 3-4, 300-311. doi:
661 10.1016/j.tecto.2009.02.047.
662 Palano, M., 2016. Episodic slow slip events and seaward flank motion at Mt. Etna volcano
663 (Italy), Journal of Volcanology and Geothermal Research, Volume 324, 15 September 2016, Pages
664 8-14, ISSN 0377-0273, doi: 10.1016/j.jvolgeores.2016.05.010.
665 Patanè, D., Privitera, E., Gresta, S., Alparone, S., Akinci, A., Barberi, G., Chiaraluce, L.,
666 Cocina, O., D'Amico, S., De Gori, P., Di Grazia, G., Falsaperla, S., Ferrari, F., Gambino, S.,
667 Giampiccolo, E., Langer, H., Maiolino, V., Moretti, M., Mostaccio, A., Musumeci, C., Piccinini,

668 D., Reitano, D., Scarfì, L., Spampinato, S., Ursino, A., Zuccarello, L., 2003. Seismological
669 constraints for the dyke emplacement of the July-August 2001 lateral eruption at Mt. Etna volcano,
670 Italy . Ann. of Geophysics, 46, 599-608, doi: 10.4401/ag-6302.
671 Patanè, D., Mattia, M., Aloisi, M., 2005. Shallow intrusive processes during 2002-2004 and
672 current volcanic activity on Mt. Etna. Geophys. Res. Lett., 32, p. L06302. doi:
673 10.1029/2004GL021773.
674 Privitera, E., Bonanno, A., Gresta, S., Nunnari, G., Puglisi, G., 2012. Triggering mechanisms of
675 static stress on Mount Etna volcano. An application of the boundary element method. J. Volcanol.
676 Geotherm. Res., 245–246 (2012), pp. 149–158. doi:10.1016/j.jvolgeores.2012.08.012.
677 Pulvirenti, F., Aloisi, M., Jin, S., 2016. Time-dependent Coulomb stress changes induced by the
678 2002-2003 Etna magmatic intrusions and implications on following seismic activities. Journal of
679 Volcanology and Geothermal Research. doi: 10.1016/j.jvolgeores.2016.11.001.
680 Reasenberg, P.A., Oppenheimer, D., 1985. FPFIT, FPPLOT and FPPAGE: fortran computer
681 progams for calculating and displaying earthquake fault-plane solutions, Open File Rep., 85-379,
682 109 pp., U. S. Geol. Surv., Washington.
683 Reasenberg, P.A., Simpson R.W., 1992. Response of regional seismicity to the static stress
684 change produced by the Loma Prieta earthquake, Science, 255, 5052, 1687-1690. doi:
685 10.1126/science.255.5052.1687.
686 Ruch, J., Pepe, S., Casu, F., Solaro, G., Pepe, A., Acocella, V., Neri, M., Sansosti, E., 2013.
687 Seismo-tectonic behavior of the Pernicana Fault System (Mt Etna): A gauge for volcano flank
688 instability?, J. Geophys. Res. Solid Earth, 118, 4398–4409, doi:10.1002/jgrb.50281.
689 Siniscalchi, A., Tripaldi, S., Neri, M., Giammanco, S., Piscitelli, S., Balasco, M., Behncke, B.,
690 Magrì, C., Naudet, V., Rizzo, E., 2010. Insights into fluid circulation across the Pernicana Fault
691 (Mt. Etna, Italy) and implications for flank instability, Journal of Volcanology and Geothermal
692 Research, Volume 193, Issues 1–2, Pages 137-142, ISSN 0377-0273, doi:
693 10.1016/j.jvolgeores.2010.03.013.

694 Siniscalchi, A., Tripaldi, S., Neri, M., Balasco, M., Romano, G., Ruch, J., Schiavone, D., 2012.
695 Flank instability structure of Mt. Etna inferred by a magnetotelluric survey, J. Geophys. Res., 117,
696 B03216, doi:10.1029/2011JB008657.
697 Stein, R. S. 1999. The role of stress transfer in earthquake occurrence, Nature, 402, 605-609.
698 doi:10.1038/45144.
699 Thatcher, W., Savage, J.C., 1982. Triggering of large earthquakes by magma-chamber inflation,
700 Izu Peninsula, Japan, Geology, 10 (12), 637-640. doi: 10.1130/0091-7613.
701 Tiampo K. F., Rundle J. B., Fernandez J. and J. O. Langbein, 2000. Spherical and ellipsoidal
702 volcanic sources at Long Valley caldera, California, using a genetic algorithm inversion technique.
703 J. Volcanol. Geotherm. Res., 102, 189-206, doi: 10.1016/S0377-0273(00)00185-2.
704 Toda, S., Stein, R.S., Sagiya, T, 2002. Evidence from the AD 2000 Izu islands earthquake
705 swarm that stressing rate governs seismicity. Nature 419, 58–61, doi:10.1038/nature00997.
706 Toda, S., Stein R.S., Lin, J., 2011. Widespread seismicity excitation throughout central Japan
707 following the 2011 M=9.0 Tohoku earthquake and its interpretation by Coulomb stress transfer.
708 Geophysical Research Letters, 38, 7. doi: 10.1029/2011GL047834.
709 Walter, T. R., Amelung, F., 2004. Influence of volcanic activity at Mauna Loa, Hawaii, on
710 earthquake occurrence in the Kaoiki Seismic Zone, Geophys. Res. Lett., 31, L07622,
711 doi:10.1029/2003GL019131.
712 Williams, C. A., and G. Wadge, 2000. An accurate and efficient method for including the
713 effects of topography in three-dimensional elastic models of ground deformation with applications
714 to radar interferometry, J. Geophys. Res., 105(B4), 8103–8120, doi:10.1029/1999JB900307.
715 Xu, C., Wang, J., Li, Z., Drummond, J., 2010. Applying the Coulomb failure function with an
716 optimally oriented plane to the 2008 Mw 7.9 Wenchuan earthquake triggering, Tectonophysics,
717 Volume 491, Issues 1–4, Pages 119-126, ISSN 0040-1951, doi: 10.1016/j.tecto.2009.09.019.

718 Yang X. M., P. M. Davis and J. H. Dieterich, 1988. Deformation from inflation of a dipping
719 finite prolate spheroid in an elastic half-space as a model for volcanic stressing, J. Geophys. Res.,
720 93, 4249–4257.
721
722
723
724
725
726
727
728
729
730
731
732
733
734
735
736
737
738
739
740
741
742
743

Figure 1

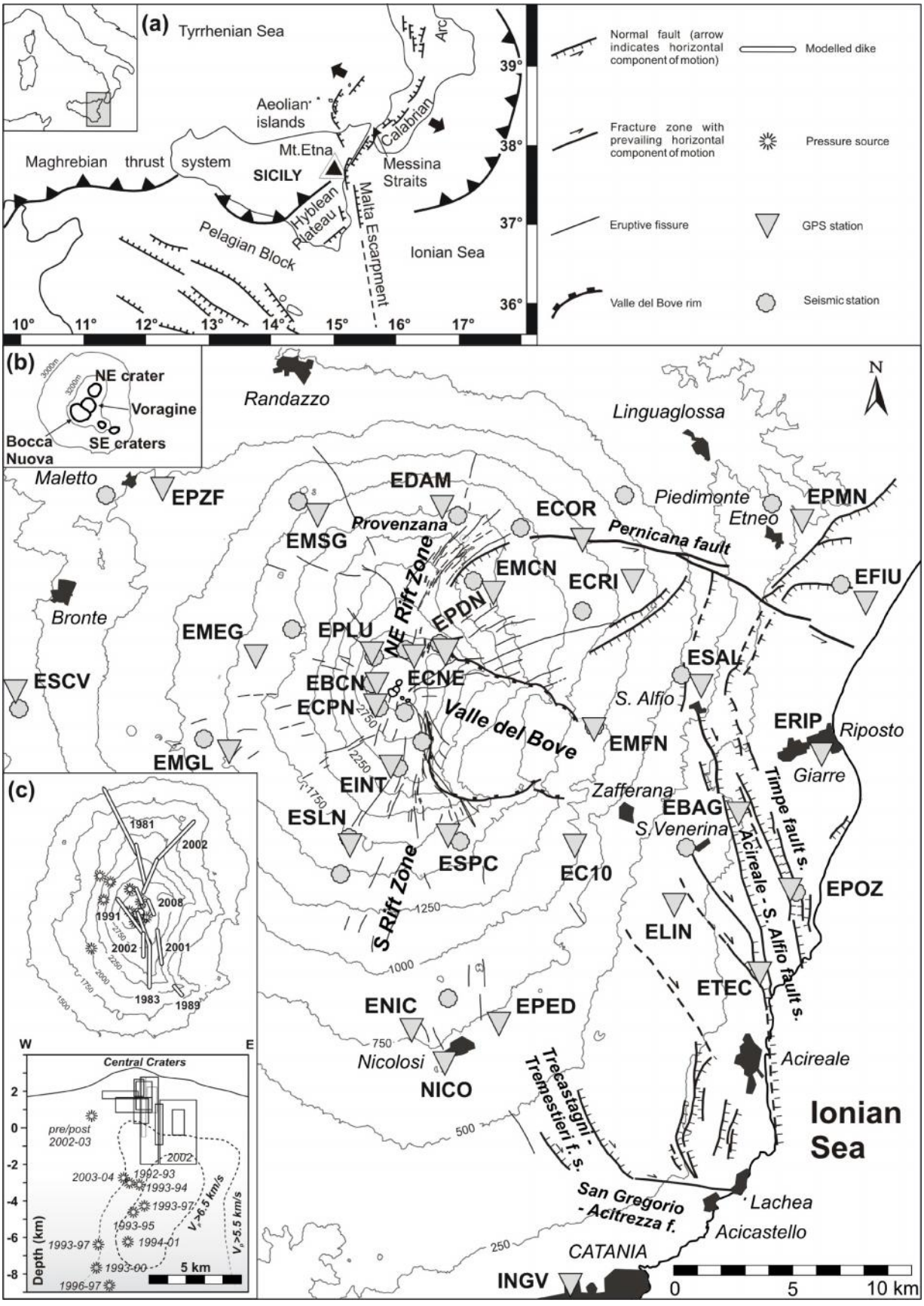
(a)
Tyrrhenian Sea
Aeolian islands
Mt.Etna
SICILY
Maghrebian thrust system
Calabrian Arc
Messina Straits
Hyblean Plateau
Malta Escarpment
Pelagian Block
Ionian Sea
39°
38°
37°
36°
10°
11°
12°
13°
14°
15°
16°
17°
Normal fault (arrow indicates horizontal component of motion)
Modelled dike
Fracture zone with prevailing horizontal component of motion
Pressure source
Eruptive fissure
GPS station
Valle del Bove rim
Seismic station
(b)
NE crater
Voragine
Bocca Nuova
SE craters
3000m
3500m
N
Randazzo
Linguaglossa
Maletto
Piedimonte Etneo
Bronte
Provenzana
Pernicana fault
NE Rift Zone
Valle del Bove
S. Alfio
Zafferana
S.Venerina
Riposto
Giarre
Timpe fault s.
Acireale - S. Alfio fault s.
S Rift Zone
Trecastagni - Tremestieri f. s.
San Gregorio - Acitrezza f.
Acireale
Lachea
Acicastello
CATANIA
Nicolosi
Ionian Sea
EPZF
EDAM
EMSG
ECOR
EPMN
EMCN
ECRI
EFIU
EPDN
EMEG
EPLU
ESAL
ESCV
EBCN
ECNE
ECPN
ERIP
EMFN
EMGL
EINT
EBAG
ESLN
ESPC
EC10
EPOZ
ELIN
ETEC
ENIC
EPED
NICO
INGV
2750
2250
1750
1250
1000
750
500
250
0
5
10 km
(c)
1981
2002
2008
1991
2001
1983
1989
W
E
Central Craters
pre/post 2002-03
2003-04
1992-93
1993-94
1993-97
1993-95
1994-01
1993-00
1996-97
Depth (km)
5 km
Vp>6.5 km/s
Vp>5.5 km/s

770 Figure 2

771

772

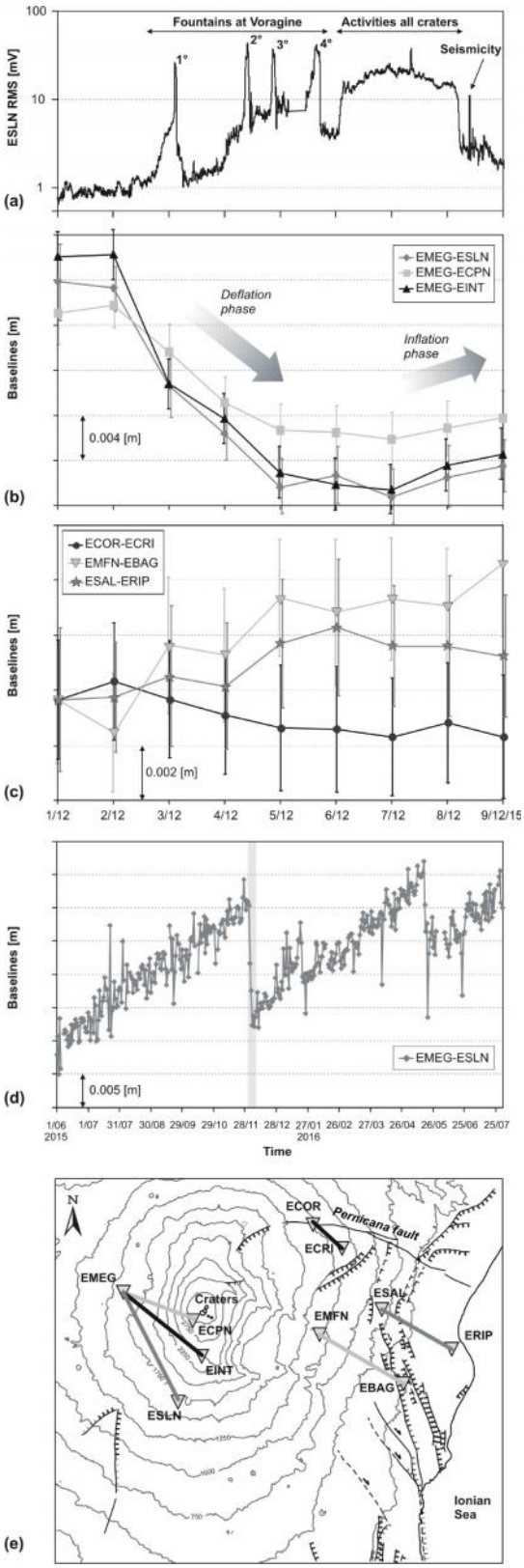

795

Figure 3

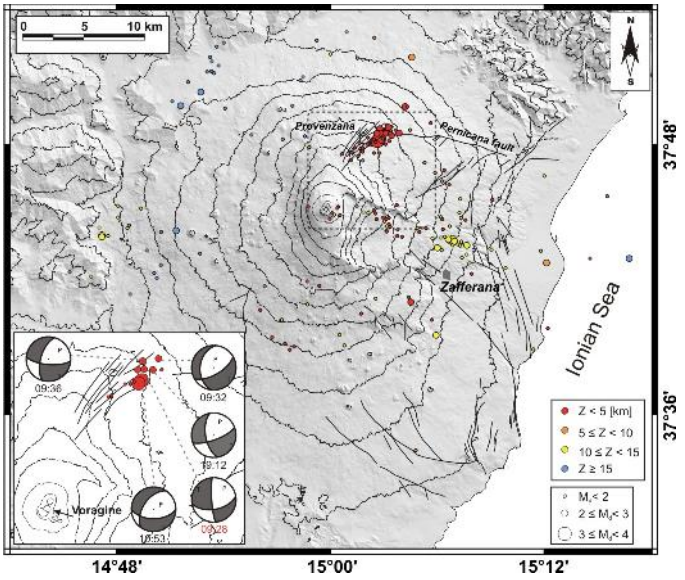
0 5 10 km
N
S
Provenzana
Pernicana fault
Zafferana
Ionian Sea
37°48'
37°36'
14°48'
15°00'
15°12'
09:36
09:32
09:12
Voragine
10:53
09:28
Z < 5 [km]
5 ≤ Z < 10
10 ≤ Z < 15
Z ≥ 15
M_d < 2
2 ≤ M_d < 3
3 ≤ M_d < 4

Figure 4

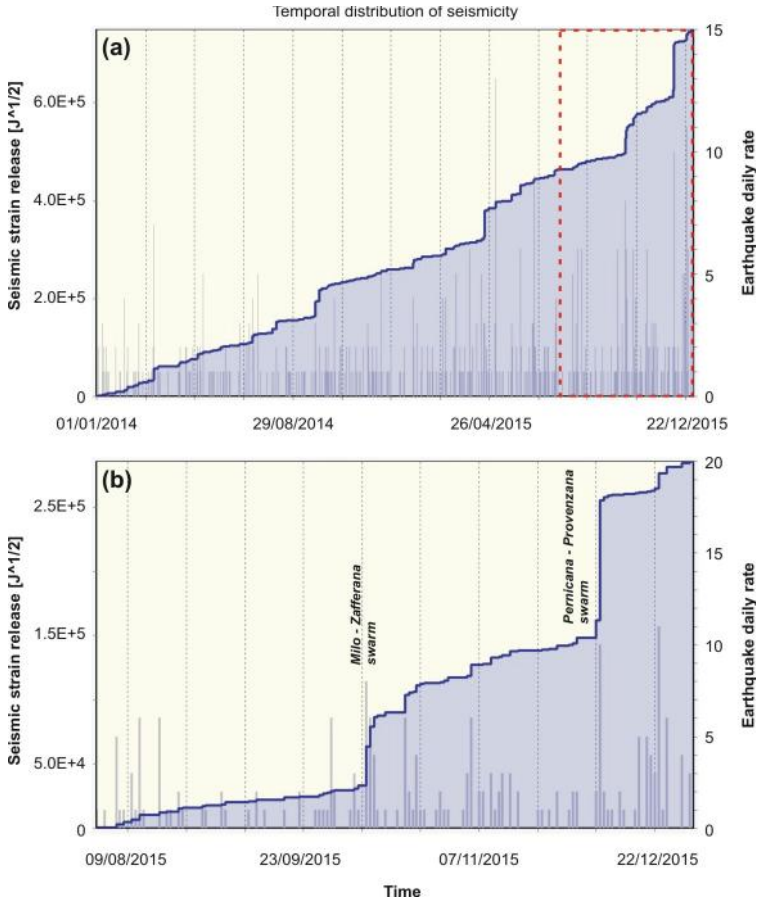
Temporal distribution of seismicity
(a)
Seismic strain release [J^1/2]
6.0E+5
4.0E+5
2.0E+5
0
Earthquake daily rate
15
10
5
0
01/01/2014
29/08/2014
26/04/2015
22/12/2015
(b)
Seismic strain release [J^1/2]
2.5E+5
1.5E+5
5.0E+4
0
Milo - Zafferana swarm
Pernicana - Provenzana swarm
Earthquake daily rate
20
15
10
5
0
09/08/2015
23/09/2015
07/11/2015
22/12/2015
Time

Figure 5

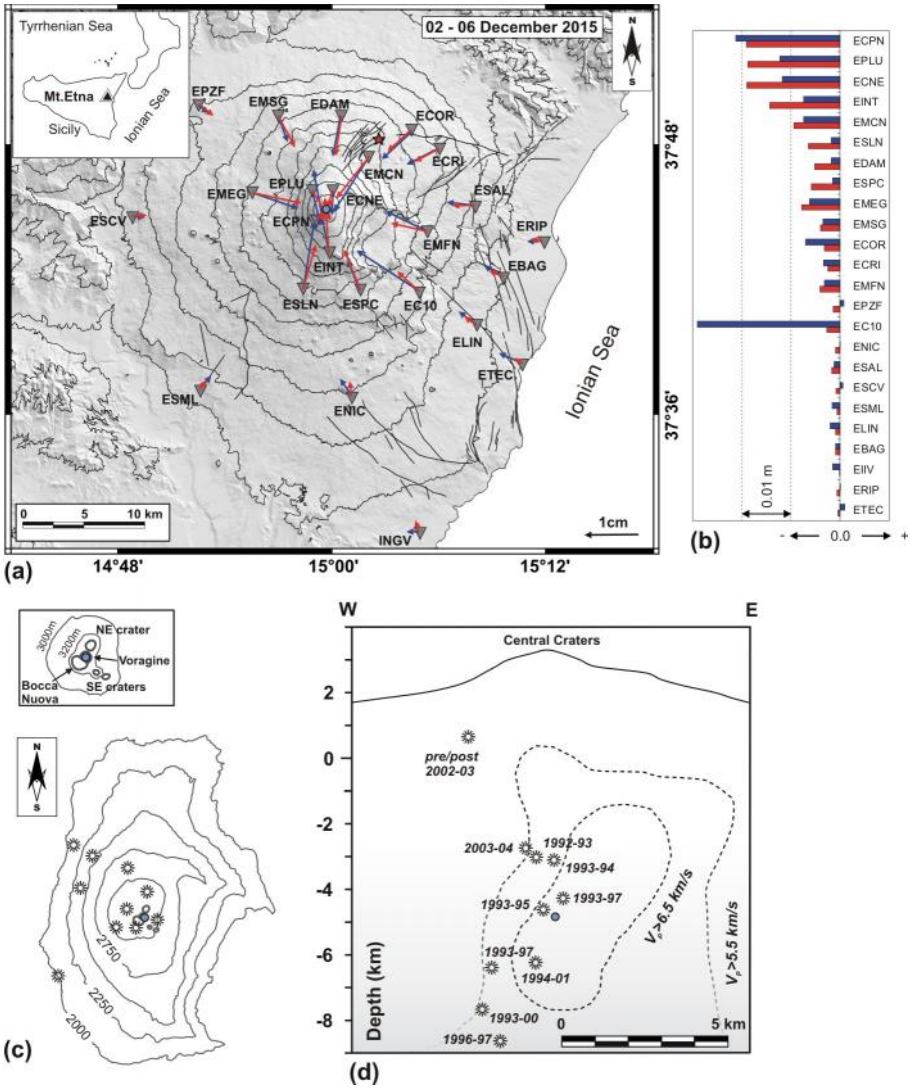
Tyrrhenian Sea
Mt.Etna
Sicily
Ionian Sea
02 - 06 December 2015
EPZF
EMSG
EDAM
ECOR
ECRI
EMCN
EPLU
EMEG
ECNE
ESAL
ESCV
ECPN
ERIP
EMFN
EBAG
EINT
ESLN
ESPC
EC10
ELIN
ETEC
ESML
ENIC
INGV
Ionian Sea
37°48'
37°36'
14°48'
15°00'
15°12'
0 5 10 km
1cm
(a)
ECPN
EPLU
ECNE
EINT
EMCN
ESLN
EDAM
ESPC
EMEG
EMSG
ECOR
ECRI
EMFN
EPZF
EC10
ENIC
ESAL
ESCV
ESML
ELIN
EBAG
EIIV
ERIP
ETEC
0.01 m
0.0
(b)
3000m
3200m
NE crater
Voragine
Bocca Nuova
SE craters
2750
2250
2000
(c)
W
E
Central Craters
pre/post 2002-03
2003-04
1992-93
1993-94
1993-95
1993-97
1993-97
1994-01
1993-00
1996-97
V_p>6.5 km/s
V_p>5.5 km/s
Depth (km)
2
0
-2
-4
-6
-8
0
5 km
(d)

841 Figure 6

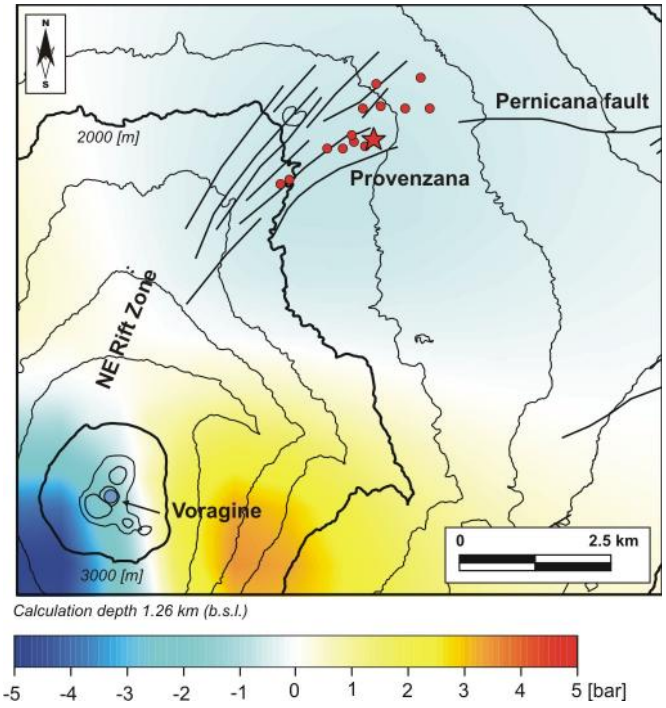

842

843

844

845

846

847

848

849

850

851

852

853

854

855

856

857

858 Figure 7

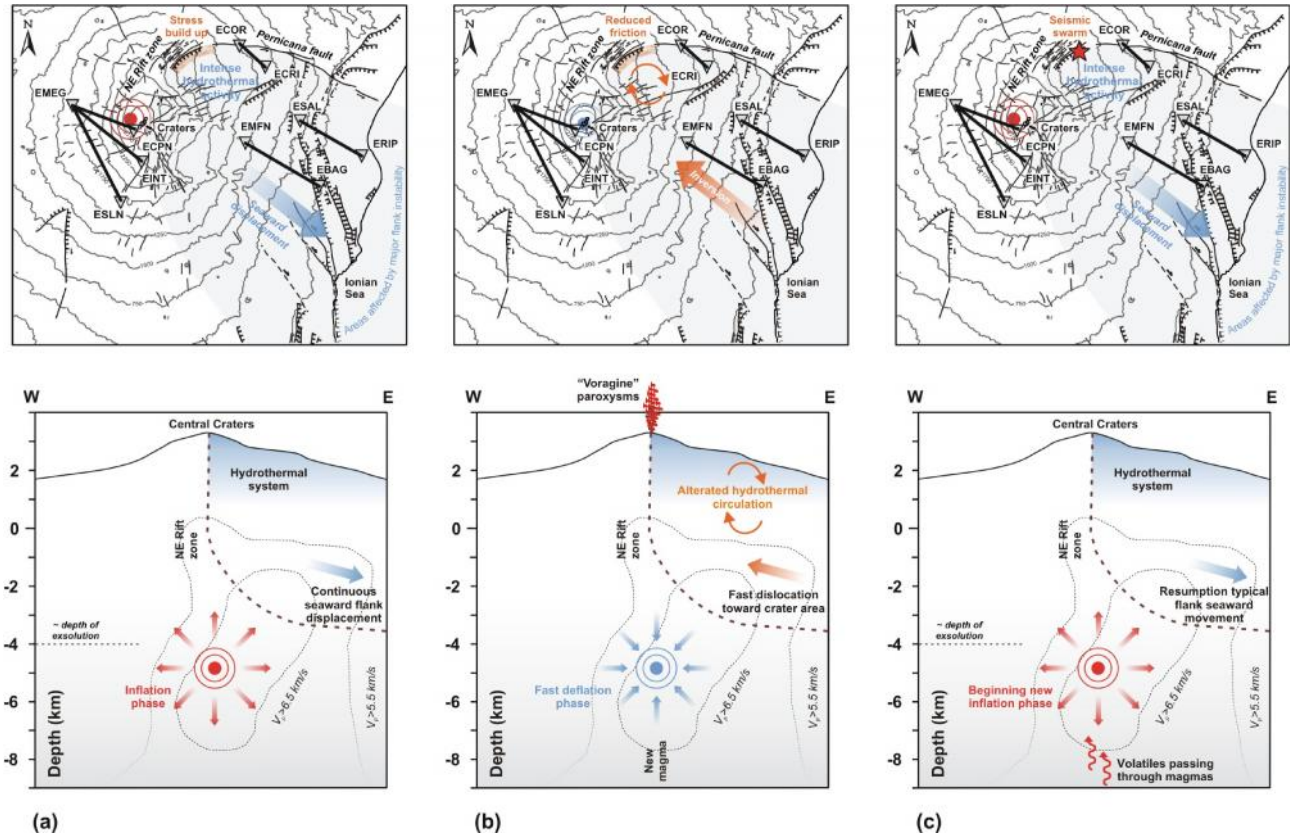

859